Poly(3,4-ethylenediselena)thiophene—The Selenium Equivalent of PEDOT

Hao Pang,[†] Peter J. Skabara,*[,†] Sergey Gordeyev,[†] Joseph J. W. McDouall,[‡] Simon J. Coles,[§] and Michael B. Hursthouse[§]

WestCHEM, Department of Pure and Applied Chemistry, University of Strathclyde, Glasgow G1 1XL, United Kingdom, School of Chemistry, University of Manchester, Manchester M13 9PL, United Kingdom, and Department of Chemistry, University of Southampton, Highfield, Southampton SO17 1BJ, United Kingdom

Received September 19, 2006. Revised Manuscript Received October 31, 2006

The first synthesis of the selenium analogue of EDOT, together with its electrochemical polymerization and redox and electronic properties of the resulting polymer, poly(3,4-ethylenediselena)thiophene (PEDST), is reported. The HOMO and LUMO values for the polymer (calculated from cyclic voltammetry experiments) are −4.8 and −3.3 eV, respectively, whereas the experimental band gap is 1.55 eV. Within the related series of polymers—PEDOT, PEDTT, and PEDST—the selenium analogue has a significantly lower LUMO value than the oxygen or sulfur derivatives (by ca. 0.55 eV). Quantum chemical calculations on trimers ($(EDXT)_3$, where X = O, S, or Se) show that the most planar conformation within the conjugated chain is achieved by EDOT systems. However, the calculated energy of a fixed planar conformation for PEDST is 13.9 kJ mol^{-1} lower than the corresponding unconstrained conformer, indicating that a planar structure is preferred; this data corroborates the lower experimental band gap observed for PEDST (1.55 eV) compared to PEDTT (2.19 eV).

Introduction

Phenomenal interest in the conjugated polymer poly(3,4-dioxyethylene)thiophene, PEDOT, as a material in organic semiconductor electronic devices has fostered the investigation of many variants.[1] For example, the EDOT unit has been used as a component in many molecular-based materials and copolymers. The structure of EDOT has also been manipulated to provide soluble analogues of PEDOT, such as the PProDOT series of polymers pioneered by Reynolds.[2−5] In a similar fashion, the oxygen atoms of PEDOT have been replaced by sulfurs to give the polymer PEDTT, which was first prepared by Kanitzidis[6] and later studied by us.[7] However, the all-sulfur analogue has strikingly different optical and redox properties compared to PEDOT, which is mainly attributable to the loss in planarity within the conjugated chain due to steric interactions between sulfur atoms in adjacent repeat units.[8] Nevertheless, PEDTT is still an attractive material in principle because of the potential number of interchain close contacts through the sulfur atoms, which should assist the charge transport properties of the polymer. Within the tetrachalcogenafulvalene family of charge-transfer materials, it is well-established that replacement of sulfur atoms by selenium raises the dimensionality and conductivity of the materials substantially, which is due to the stronger nature of intermolecular contacts between Se atoms and their greater stabilization effects toward radical cations.[9,10] Similarly, we and others have found increased mobilities in selenophene-based materials compared to the corresponding thiophene analogues.[11−13] To this end, an investigation into the selenium variant of EDOT is highly appealing. Herein, we report the first synthesis and isolation of (3,4-ethylenediselena)thiophene (EDST), its polymerization, and the optical and redox properties of the polymer PEDST.

Experimental Section

General. Melting points were taken using a Stuart Scientific SMP1 melting point apparatus and are uncorrected. ^1H and ^{13}C NMR spectra were recorded on a Bruker DPX instrument at 400 and 100 MHz; chemical shifts are given in parts per million. IR

* Corresponding author. E-mail: peter.skabara@strath.ac.uk.
[†] University of Strathclyde.
[‡] University of Manchester.
[§] University of Southampton.

(1) Kirchmeyer, S.; Reuter, K. *J. Mater. Chem.* **2005**, *15*, 2077.
(2) Gaupp, C. L.; Welsh, D. M.; Rauh, R. D.; Reynolds, J. R. *Chem. Mater.* **2002**, *14*, 3964.
(3) Schwendeman, I.; Hickman, R.; Sonmez, G.; Schottland, P.; Zong, K.; Welsh, D. M.; Reynolds, J. R. *Chem. Mater.* **2002**, *14*, 3118.
(4) Cirpan, A.; Argun, A. A.; Grenier, C. R. G.; Reeves, B. D.; Reynolds, J. R. *J. Mater. Chem.* **2003**, *13*, 2422.
(5) Aubert, P. H.; Argun, A. A.; Cirpan, A.; Tanner, D. B.; Reynolds, J. R. *Chem. Mater.* **2004**, *16*, 2386.
(6) Wang, C. G.; Schindler, J. L.; Kannewurf, C. R.; Kanatzidis, M. G. *Chem. Mater.* **1995**, *7*, 58.
(7) Spencer, H. J.; Skabara, P. J.; Giles, M.; McCulloch, L.; Coles, S. J.; Hursthouse, M. B. *J. Mater. Chem.* **2005**, *15*, 4783.
(8) Turbiez, M.; Frere, P.; Allain, M.; Gallego-Planas, N.; Roncali, J. *Macromolecules* **2005**, *38*, 6806.
(9) Cowan, D.; Kini, A., *The Chemistry of Organic Selenium and Tellurium Compounds*; Wiley: Chichester, U.K., 1987; Vol. 2.
(10) Bryce, M. R. *J. Mater. Chem.* **1995**, *5*, 1481.
(11) Kunugi, Y.; Takimiya, K.; Toyoshima, Y.; Yamashita, K.; Aso, Y.; Otsubo, T. *J. Mater. Chem.* **2004**, *14*, 1367.
(12) Crouch, D. J.; Skabara, P. J.; Lohr, J. E.; McDouall, J. J. W.; Heeney, M.; McCulloch, I.; Sparrowe, D.; Shkunov, M.; Coles, S. J.; Horton, P. N.; Hursthouse, M. B. *Chem. Mater.* **2005**, *17*, 6567.
(13) Kim, Y. M.; Lim, E.; Kang, I. N.; Jung, B. J.; Lee, J.; Koo, B. W.; Do, L. M.; Shim, H. K. *Macromolecules* **2006**, *39*, 4081.

10.1021/cm062242p CCC: $37.00
Published on Web 12/24/2006

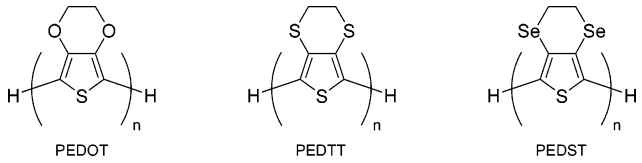

spectra for the characterization of the compounds were recorded on a Perkin−Elmer FTIR spectrometer. Mass spectra were recorded on a ThermoFinnigan LCQ DUO mass spectrometer and a Polaris Q TRACE GC 2000. Elemental analyses were obtained on a Perkin−Elmer 2400 elemental analyzer. Absorption spectra were measured on a Unicam UV 300 spectrophotometer. Electrochemical measurements were performed on a CH Instruments 660A electrochemical workstation with IR compensation using anhydrous dichloromethane or acetonitrile as the solvent, silver wire as the pseudo reference electrode, and platinum wire and glassy carbon as the counter and working electrodes, respectively. Electrochemical data were referenced to the ferrocene/ferrocenium redox couple using the metallocene as an internal standard. All solutions were degassed (Ar) and contained monomer substrates in concentrations of ca. 1×10^{-3} M, together with *n*-Bu_4NPF_6 (0.1 M) as the supporting electrolyte. Spectroelectrochemical experiments were conducted on ITO glass.

Crystal Structure Determination for 3. Data were collected at 120 K on an Nonius KappaCCD area detector diffractometer located at the window of a Nonius FR591 rotating anode X-ray generator, equipped with a molybdenum target (λ Mo−K_α = 0.71073 Å). The structure was solved and refined using the SHELX-97 suite of programs.[14] Data were corrected for absorption effects by means of comparison of equivalent reflections using the program SADABS.[15] Non-hydrogen atoms were refined anisotropically, whereas hydrogen atoms were fixed in idealized positions with their thermal parameters riding on the values of their parent atoms. $C_{20}H_{36}S_2Se_4Si_4$, M = 768.81, triclinic, a = 6.2840(2) Å, b = 9.5240(2) Å, c = 13.6870(4) Å, α = 77.853(2)°, β = 81.908(2)°, γ = 86.535(2)°, U = 792.44(4) Å^3, space group $P\bar{1}$, Z = 1, μ(Mo−K_α) = 4.921 mm^{-1}, 18 635 reflections measured, 3635 unique (R_{int} = 0.0513), which were used in all calculations. The final $wR(F^2)$ was 0.0733 (all data). Supplementary data have been deposited with the Cambridge Crystallographic Data Centre (deposition number = CCDC613197).

2,5-Bis(trimethylsilyl)-3,4-dibromothiophene (2). 2,3,4,5-Tetrabromothiophene **1** (15 g, 37.5 mmol) was added to a 250 mL three-necked flask containing anhydrous THF (80 mL) under nitrogen. The solution was cooled to −65 °C with acetone/dry ice. A solution of *n*-BuLi (2.5 M, 15 mL, 37.5 mmol in hexanes) was added dropwise over 15 min, and the mixture was stirred for half an hour. A solution of chlorotrimethylsilane (4.76 mL, 37.5 mmol) was then added in one portion and stirring was maintained for 1.5 h. An additional 1 equiv of *n*-BuLi (2.5 M, 15 mL, 37.5 mmol) was added dropwise. The solution was stirred for a further 0.5 h before a second portion of chlorotrimethylsilane (4.76 mL, 37.5 mmol) was added. After being stirred for half an hour, the reaction mixture was allowed to warm to 20 °C and left to stir overnight. After the addition of saturated ammonium chloride solution (100 mL), the mixture was extracted with dichloromethane (3 × 100 mL), and the combined organic phases were washed with water (3 × 80 mL), dried over $MgSO_4$, and evaporated under reduced pressure. The resulting colorless oil was purified by distillation (2 mm Hg, 110 °C) to give 2,5-bis(trimethylsilyl)-3,4-dibromothiophene (13.75 g, 95%). δ_H (400 MHz, $CDCl_3$, Me_4Si): 0.43 (18H, s). δ_C (100 MHz, $CDCl_3$, Me_4Si): −0.93, 122.4, 140.9. *m/z* (EI) 386 (M^+, 100%).

1,3,6,8-Tetrakis-trimethylsilanyl-2,7-dithia-4,5,9,10-tetraselena-dicyclopenta[*a,e*]cyclooctene (3). 2,5-Bis(trimethylsilyl)-3,4-dibromothiophene **2** (3.86 g, 10 mmol) was added to a 500 mL three-necked flask containing anhydrous THF (200 mL) under nitrogen. The solution was cooled to −65 °C by acetone/dry ice. A solution of *t*-BuLi (1.7 M, 12 mL, 20.5 mmol) was added dropwise over 20 min, and the mixture was stirred for 1 h. Selenium powder (0.8 g, 10 mmol) was added to the reaction system in one portion. The temperature of the reaction was kept in the range −65 to −25 °C until all the selenium powder dissolved. After cooling the reaction again to −65 °C, we added an additional 2.05 equiv of *t*-BuLi (1.7 M, 12 mL, 20.5 mmol) dropwise. The solution was stirred for a further 1 h before a second portion of dry selenium powder (0.8 g, 10 mmol) was added. The reaction system was allowed to warm to room temperature slowly and was left to stir overnight. After the addition of saturated ammonium chloride solution (100 mL), the mixture was extracted with chloroform (3 × 100 mL), and the combined organic phases were washed with water (3 × 80 mL), dried over $MgSO_4$, and evaporated under reduced pressure. The resulting orange solid was washed with methanol and purified by recrystallization from hot chloroform to give orange-red crystals (2.5 g, yield 65%). δ_H (400 MHz, $CDCl_3$, Me_4Si): 0.45 (36H, s). δ_C (100 MHz, $CDCl_3$, Me_4Si): 0.5, 142.1, 153.4. *m/z* (AP^+) 771 ($[M+H]^+$, 100%). Anal. Calcd for $C_{20}H_{36}S_2Se_4Si_4$: C, 31.25; H, 4.72. Found: C, 31.54; H, 4.71. FT−IR (powder; υ, cm^{-1}): 2951, 2896, 1410, 1325, 1251, 1004, 837. M.p. 324−325 °C.

2,5-Bis(trimethylsilyl)-3,4-ethylenediselenathiophene (4). Compound **(3)** (1.28 g, 1.67 mmol) was added to a 250 mL three-necked flask containing anhydrous THF (150 mL) under nitrogen. The solution was cooled to 0 °C, and lithium triethylborohydride (1.0 M, 6.6 mL, 6.68 mmol) was added dropwise over 10 min. After 1 h, 1,2-dibromoethane (0.29 mL, 3.34 mmol) was added in one portion; the reaction was allowed to warm to room temperature slowly and was left to stir overnight. After the addition of saturated ammonium chloride solution (100 mL), the mixture was extracted with chloroform (3 × 100 mL), and the combined organic phases were washed with water (3 × 80 mL), dried over $MgSO_4$, and evaporated under reduced pressure. The resulting orange solid was purified by column chromatography (silica, petroleum ether (bp 40−60 °C):dichloromethane, 4:1 v/v) to afford a white solid (1.30 g, 95%). δ_H (400 MHz, $CDCl_3$, Me_4Si): 0.40 (18H, s), 3.28 (4H, s). δ_C (100 MHz, $CDCl_3$, Me_4Si): −0.2, 23.9, 132.3, 140.2. Anal. Calcd for $C_{12}H_{22}SSe_2Si_2$: C, 34.94; H, 5.38. Found: C, 34.92; H, 5.22. *m/z* (EI) 413.8 (M^+, 100%), 385.9 (55%) 370.8 (35%), 355.9 (10%), 233.0 (50%). FT−IR (powder; υ, cm^{-1}): 2951, 2890, 1405, 1350, 1246, 1144, 1089, 1018, 837. M.p. 86−87 °C.

3,4-Ethylenediselenathiophene (EDST). 2,5-Bis(trimethylsilyl)-3,4-ethylenediselenathiophene (**4**) (0.635 g, 1.54 mmol) was added to a 100 mL flask containing THF (50 mL) at room temperature. A solution of tetrabutyl ammonium fluoride (TBAF) (1.0 M, 4 mL, 3.85 mmol) was added, together with a drop of water, and the reaction mixture was left to stir overnight. After the addition of saturated ammonium chloride solution (100 mL), the mixture was extracted with chloroform (3 × 100 mL), and the combined organic phases were washed with water (3 × 80 mL), dried over $MgSO_4$, and evaporated under reduced pressure. The resulting brown sticky oil was purified by column chromatography (silica, petroleum ether (bp 40−60 °C):dichloromethane, 2:1 v/v) to afford a pale yellow sticky oil that solidified after storage (0.33 g, 78%). δ_H (400 MHz, $CDCl_3$, Me_4Si): 3.23 (4H, s), 7.15 (2H, s). δ_C (100 MHz, $CDCl_3$,

(14) Sheldrick, G. M. *SHELX-97: Programs for Structure Solution and Refinement*; University of Göttingen: Göttingen, Germany, 1997.
(15) Sheldrick, G. M. *SADABS*, version 2.10; Bruker AXS, Inc.: Madison, WI, 2003.

Scheme 1

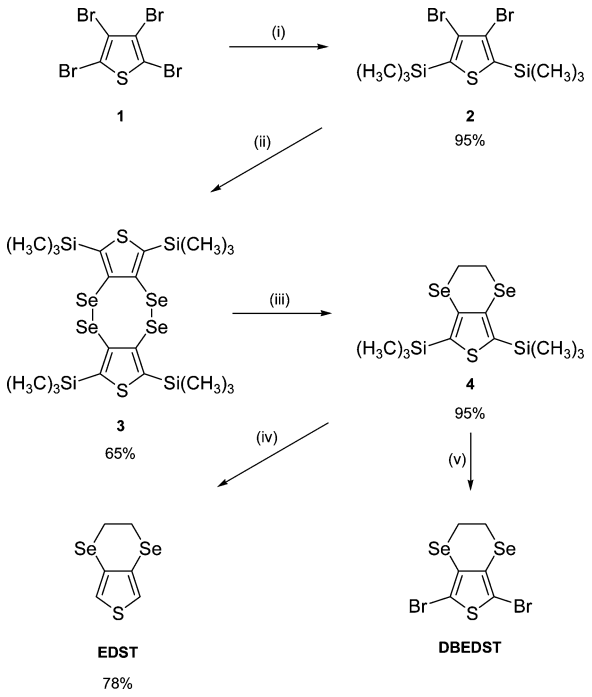

Reagents and conditions: (i) *n*-BuLi (2.5 M, 2 equiv), THF, −65 °C, 1.5 h, TMSCl (2 equiv), overnight; (ii) *t*-BuLi (1.7 M, 4 equiv), THF, Se, −25 to −65 °C to rt, overnight; (iii) super hydride (1 M, 4 equiv), THF, 0 °C to rt, 1,2-dibromoethane, overnight; (iv) TBAF (1 M, 2.5 equiv), rt, THF, overnight; (v) Br_2, CH_2Cl_2, rt.

Me_4Si): 23.5, 121.9, 121.9, 122.0. Anal. Calcd for $C_6H_6SSe_2$: C, 26.88; H, 2.26. Found: C, 27.04; H, 2.07. *m*/*z* (EI) 269.8 (M^+, 80%), 241.9 (60%). HRMS (EI) *m*/*z* calcd for $C_6H_6SSe_2$, 269.8515; found, 269.8522; FT−IR (solid; υ, cm^{-1}): 3092, 2917, 1459, 1407, 1312, 1269, 1234, 1143, 1104, 919, 897, 848, 795. M.p. 29−30 °C.

Synthesis. The synthesis of EDST is summarized in Scheme 1. Tetrabromothiophene (**1**) was lithiated using 2 equiv of *n*-butyllithium and further reacted with trimethylsilyl chloride to give compound **2** in 95% yield. The procedure we used was different from the one previously reported,[16] which results in a lower yield (45%). In our case, 1 equiv of *n*-BuLi is added to **1**, followed by 1 equiv of trimethylsilyl chloride, and the procedure is repeated. The lower yield was obtained by adding the two reagents in single 2 equiv portions. The addition of *t*-butyllithium to **2**, followed by elemental selenium, produced the cyclic diselena-bridged compound **3**. Interestingly, the same compound was obtained in identical yield (65%) in the presence of 1,2-dibromoethane, meaning that the synthesis of **4** directly from **2** was not possible. The formation of a related 3,4-diselenothiophene dimer has been postulated as a product from the reaction of triphenylphosphine with thieno[3,4-*d*]-1,3-diselenole-2-selone, but the dimer could not be isolated.[17] However, analogous compounds have been prepared and isolated: the treatment of 4,7-diisopropyl-2,2-dimethyl-l,3,2-benzodiselenastannoles with *n*-BuLi, followed by acidification and air oxidation, gave compound **5**,[18] whereas the reaction of 2,2′-dilithio-1,1′-binaphthyl with selenium followed by air oxidation afforded **6**.[19]

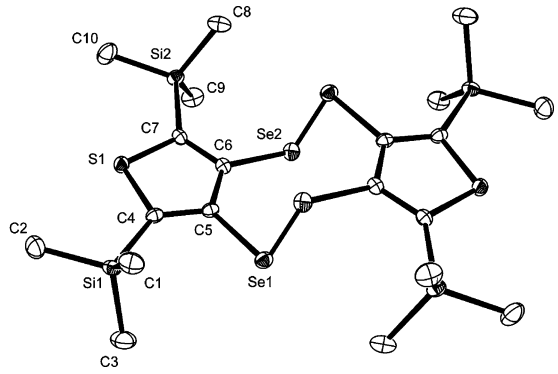

Figure 1. X-ray crystal structure of compound **3** with H atoms omitted.

Cleavage of the diselena bonds was achieved by treatment with super hydride and, in this case, the intermediate diselenide was able to react with 1,2-dibromoethane to afford compound **4** in 95% yield. Finally, the trimethylsilyl groups were removed using tetrabutyl ammonium fluoride to give the target compound EDST in 78% yield. It is worth noting that the direct bromination of compound **4** in CH_2Cl_2 led to the formation of 2,5-dibromo-3,4-ethylenediselenathiophene (DBEDST). GC mass spectrometry identified the molecular ion peak for this product but, upon removal of the solvent, the material darkened immediately and the resulting product was intractable. We attribute this observation to the spontaneous polymerization of the monomer, which has been observed (albeit at a far slower rate) for the oxygen (DBEDOT)[20,21] and sulfur (DBEDTT)[22] analogues. Attempts to isolate DBEDST at lower temperatures are under way.

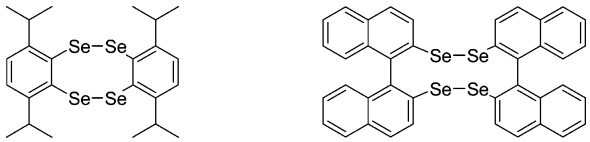

Results and Discussion

X-ray Crystallography. The structure of compound **3** was verified by X-ray crystallography and is shown in Figure 1 (see Table 1 for selected bond lengths and angles). The compound crystallizes in the $P\bar{1}$ space group, and the asymmetric unit identifies an inversion center within the plane of selenium atoms. The eight-membered ring containing the four Se atoms adopts a chair conformation with Se−Se bond lengths of 2.333(3) Å. This distance implies Se−Se single-bond character, and the C−Se bond lengths (C(5)−Se(1) = 1.912(3) Å; C(6)−Se(2) = 1.903(3) Å) are also indicative of single bonds.[23] The intramolecular nonbonded Se···Se distance across this ring is 3.624(6)Å, and due to the centrosymmetric nature of the molecular structure, the thiophene rings are perfectly parallel with respect to each other. The packing diagram of **3** is shown in Figure 2. Chains of molecules are linked together by close intermolecular Se·

(16) Lukevics, E.; Arsenyan, P.; Belyakov, S.; Popelis, J.; Pudova, O. *Tetrahedron Lett.* **2001**, *42*, 2039.
(17) Chiang, L. Y.; Shu, P.; Holt, D.; Cowan, D. *J. Org. Chem.* **1983**, *48*, 4713.
(18) Ogawa, S.; Sugawara, M.; Kawai, Y.; Niizuma, S.; Kimura, T.; Sato, R. *Tetrahedron Lett.* **1999**, *40*, 9101.
(19) Murata, S.; Suzuki, T.; Yanagisawa, A.; Suga, S. *J. Heterocycl. Chem.* **1991**, *28*, 433.
(20) Meng, H.; Perepichka, D. F.; Bendikov, M.; Wudl, F.; Pan, G. Z.; Yu, W. J.; Dong, W. J.; Brown, S. *J. Am. Chem. Soc.* **2003**, *125*, 15151.
(21) Meng, H.; Perepichka, D. F.; Wudl, F. *Angew. Chem., Int. Ed.* **2003**, *42*, 658.
(22) Spencer, H. J.; Berridge, R.; Crouch, D. J.; Wright, S. P.; Giles, M.; McCulloch, I.; Coles, S. J.; Hursthouse, M. B.; Skabara, P. J. *J. Mater. Chem.* **2003**, *13*, 2075.
(23) Oilunkaniemi, R.; Laitinen, R. S.; Ahlgren, M. *Z. Naturforsch., B: Chem. Sci.* **2000**, *55*, 361.

Table 1. Selected Geometric Parameters for Compound 3 (Å, deg)[a]

C4−C5^i	1.374(4)	C7−S1	1.727(3)
C4−S1	1.728(3)	C5−C4^i	1.374(4)
C6−C7	1.376(4)	C5−C6^i	1.435(4)
C6−C5^i	1.435(4)	C5−Se1	1.912(3)
C6−Se2	1.903(3)	Se1−Se2^i	2.333(3)
C5^i−C4−S1	108.75(19)	C7−S1−C4	94.90(13)
C5^i−C4−Si1	131.73(22)	C5−Se1−Se2	99.67(8)
S1−C4−Si1	119.49(15)	C6−Se2−Se1	100.78(8)
C7−C6−C5^i	113.81(23)	C4^i−C5−C6^i	113.81(25)
C7−C6−Se2	121.13(20)	C4^i−C5−Se1	121.22(19)
C5^i−C6−Se2	124.93(21)	C6^i−C5−Se1	124.96(19)
C6−C7−S1	108.7(2)	S1−C7−Si2	120.27(16)
C6−C7−Si2	130.98(20)		

[a] *i* denotes atoms that are generated by the symmetry operations of the space group.

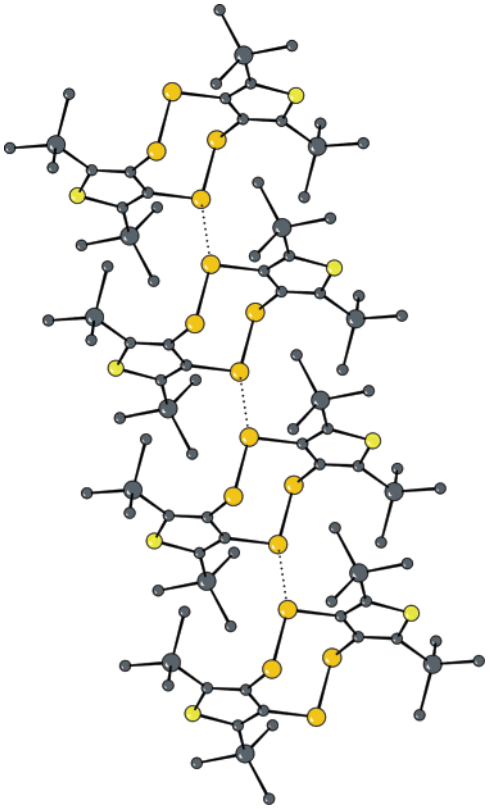

Figure 2. Packing in compound **3** viewed along the *b*-axis and showing close intermolecular Se···Se contacts.

··Se contacts. The distance between Se(1) atoms is 3.298(3) Å, which is much smaller than the sum of the van der Waals radii for two selenium atoms (3.80 Å).[24] There are no further close intermolecular contacts in the structure.

Electrochemistry. Cyclic voltammetry experiments show that the EDST monomer is irreversibly oxidized at +0.85 V (vs ferrocene in CH_2Cl_2). Repetitive cycling over this peak results in the growth of PEDST on the electrode (Figure 3; polymer deposited on glassy carbon). The emergence of a new, reversible oxidation peak at ca. +0.6 V represents the electroactivity of the depositing polymer; the full cyclic voltammogram of PEDST can be seen in Figure 4 (the solid-state experiment was run in monomer-free acetonitrile solution with $TBAPF_6$ (0.1 M) as the supporting electrolyte). Oxidation of the polymer occurs at +0.27 V, and the process is quasireversible. A single, irreversible reduction peak is

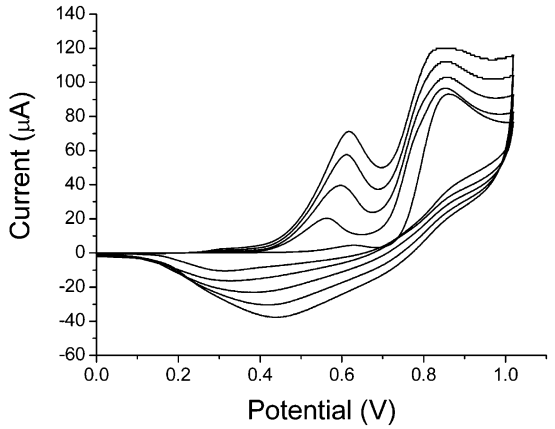

Figure 3. Electrochemical growth of PEDST on a glassy carbon working electrode in CH_2Cl_2 (1×10^{-3} M solution with 0.1 M $TBAPF_6$ as supporting electrolyte). The data is referenced to the Fc/Fc^+ redox couple.

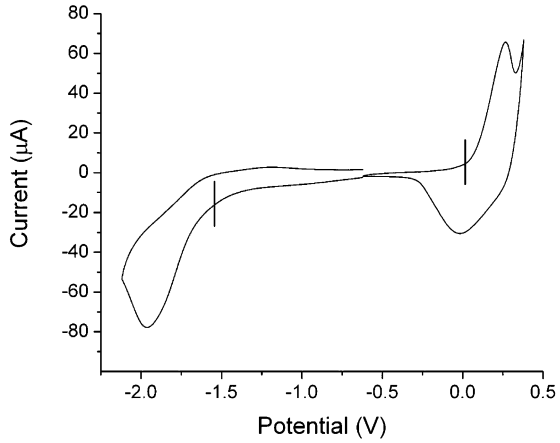

Figure 4. Cyclic voltammogram of PEDST as a thin film on a glassy carbon working electrode in monomer-free CH_3CN (0.1 M $TBAPF_6$ as supporting electrolyte). The data is referenced to the Fc/Fc^+ redox couple.

detected at −1.96 V (vs Fc/Fc^+). The onsets of the redox processes correspond to a HOMO of −4.8 eV and a LUMO of −3.3 eV (HOMO of ferrocene is taken as −4.8 eV), giving an electrochemical band gap of 1.55 eV. The latter value is much closer to that of PEDOT than PEDDT (see Table 2).[7] Although the HOMO of PEDST is similar to that of PEDTT, the LUMO is considerably lower than either of its analogues due to the increased polarizability of the selenium atom compared to oxygen and sulfur. This indicates that PEDST should be the most efficient electron-transport material in the series.

PEDST was harvested from the working electrode by gentle scraping, and the conductivity of the dark material was measured using the two-probe compressed pellet method.[25] The conductivity of the as-grown polymer (i.e. before dedoping) was found to be 3×10^{-4} S cm^{-1}.

Absorption Spectroscopy. The absorption maxima for the monomers EDOT, EDTT, and EDST (258, 289, and 282 nm, respectively) represent the substituent effects of the different chalcogen atoms toward the $\pi-\pi^*$ transition. It is clear from Table 2 that the longest wavelength absorption maxima for the polymers give the reverse trend, which is attributed to the increasing planarity of the polymer chains (PEDOT >

(24) Bondi, A. *J. Phys. Chem.* **1964**, *68*, 441.

(25) Wudl, F.; Bryce, M. R. *J. Chem. Educ.* **1990**, *67*, 717.

Table 2. Electrochemical and Electronic Absorption Data for Polymers[a]

polymer	HOMO (eV)	LUMO (eV)	E_g (eV)	λ_{max} (nm)
PEDOT	−4.0	−2.7	1.35,[b] 1.63[c]	578
PEDTT	−4.9	−2.75	2.19,[b] 2.15[c]	441
PEDST	−4.8	−3.3	1.55,[b] 1.79[c]	459

[a] Absorption spectra were taken from thin films. Data for PEDOT and PEDTT are reproduced from ref 7. [b] Electrochemical band gap. [c] Optical band gap.

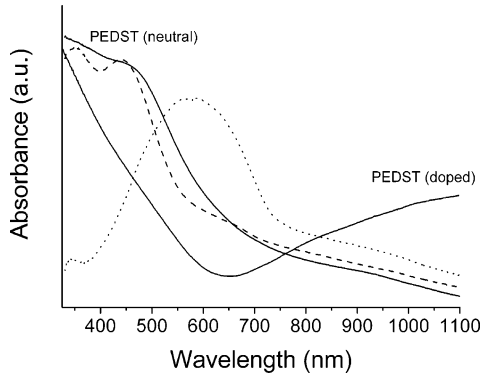

Figure 5. Absorption spectra (thin film) for PEDOT (dotted line), PEDTT (dashed line) and PEDST (solid line). The spectrum of PEDST in the doped state was recorded at +0.5 V and that in the neutral state at −0.6 V (vs Fc/Fc^+).

PEDST > PEDTT, spectra obtained from thin films). In relation to this, we and others have highlighted the importance of intrachain chalcogen−chalcogen contacts between repeat units in forming planar conformations.[7,8] The S···S interactions in PEDTT are influenced by steric repulsion, which twists the repeat units out of coplanarity; this is the main reason for the large difference in band gaps between PEDTT and PEDOT. However, the difference in λ_{max} between PEDTT and PEDST is only 18 nm, yet there is a large discrepancy in the values of E_g (0.36 eV from the absorption spectra). The tails of the longest wavelength absorption bands for all three polymers extend over several hundred nanometres (Figure 2), but it can be seen that the tail for PEDST extends further than PEDTT by ca. 100 nm. One of the contributing factors to the variation of E_g in conjugated polymers is the degree of interchain interactions.[26] It is likely that the discrepancy in band gaps between PEDTT and PEDST is partly due to the stronger interchain Se···Se contacts, in addition to planarity and substituents effects.

UV−vis spectroelectrochemistry of PEDST shows the expected disappearance of the $\pi-\pi^*$ band and the evolution of a broad band in the red to near-IR region (660−1100 nm) upon oxidation (see Figure 5). The latter is due to the signature of polaron and/or bipolaron species in the polymer. The optical transparency of the doped state in the visible region is inferior to that of PEDOT, which adopts a "bleached" appearance in its oxidized form.

Computational Chemistry. Quantum chemical calculations were performed on the trimers: $(EDOT)_3$, $(EDTT)_3$, and $(EDST)_3$ using the Gaussian 03 suite of programs.[27] One-dimensional band structure calculations were carried out on PEDOT, PEDTT, and PEDST. All structures were submitted for full geometry optimization. The 6-31G(d) basis set was used in all calculations reported here. Test calculations with the larger 6-311G(2d) basis showed very little difference in predicted band gaps and so the smaller basis was employed. A large number of exchange-correlation functionals were tested. We found that pure density functionals generally predicted band gaps that were too narrow. The hybrid B3LYP functional appears to perform best, and all calculations reported here employed this functional. Key results are displayed in Table 3.

Table 3. Key Results from B3LYP/6-31G(d) Calculations on $(EDOT)_3$, $(EDTT)_3$, $(EDST)_3$, and PEDOT, PEDTT

	δ[a] (deg)	S−X[b] (Å)	$E_{LUMO}-E_{HOMO}$ (eV)
$(EDOT)_3$	178	2.96	3.30
PEDOT	179	2.94	1.83
PEDOT (planar constraint)	180	2.94	1.84
experimental			1.63
$(EDTT)_3$	89	4.09	4.70
PEDTT	127	3.44	3.12
PEDTT (planar constraint)	180	2.98	2.07
experimental			2.15
$(EDST)_3$	128	3.35	3.69
PEDST	142	3.40	2.67
PEDST (planar constraint)	180	3.18	1.86
experimental			1.79

[a] δ is the dihdral angle between the planes of the thiophene units. [b] S−X is the contact distance between the S atom of the thiophene unit and the substituent chalcogen atom of the neighboring unit.

Geometry optimization at the B3LYP/6-31G(d) level predicts a highly planar structure for $(EDOT)_3$, with a dihedral angle between the planes of the thiophene units of 178°. In $(EDTT)_3$, these angles are 89°, giving a highly nonplanar structure. In $(EDST)_3$, the dihedral angle opens to 128°; however, the structure is far from planar. We repeated the geometry optimizations starting from planar structures, but in all cases, the same structures were obtained.

Another geometrical feature of interest is the contact distance between the S atom of the central thiophene unit and the chalcogen atoms of the exterior six-membered rings. These distances are 2.96, 4.09, and 3.35 Å in $(EDOT)_3$, $(EDTT)_3$, and $(EDST)_3$, respectively. Taking as van der Waals radii the values 1.40 (O), 1.85 (S), and 2.00 Å (Se), we observe that these contact distances are less than the sum of van der Waals radii in $(EDOT)_3$ and $(EDST)_3$, but in $(EDTT)_3$, the contact distance exceeds the sum of van der Waals radii. Noncovalent interactions are not well-described within a density functional formalism. To provide quantitative evidence for the function of the close contacts, we must

(26) Roncali, J. *Chem. Rev.* **1997**, *97*, 173.

(27) All calculations were performed using: Frisch, M. J.; Trucks, G. W.; Schlegel, H. B.; Scuseria, G. E.; Robb, M. A.; Cheeseman, J. R.; Montgomery, J. A., Jr.; Vreven, T.; Kudin, K. N.; Burant, J. C.; Millam, J. M.; Iyengar, S. S.; Tomasi, J.; Barone, V.; Mennucci, B.; Cossi, M.; Scalmani, G.; Rega, N.; Petersson, G. A.; Nakatsuji, H.; Hada, M.; Ehara, M.; Toyota, K.; Fukuda, R.; Hasegawa, J.; Ishida, M.; Nakajima, T.; Honda, Y.; Kitao, O.; Nakai, H.; Klene, M.; Li, X.; Knox, J. E.; Hratchian, H. P.; Cross, J. B.; Adamo, C.; Jaramillo, J.; Gomperts, R.; Stratmann, R. E.; Yazyev, O.; Austin, A. J.; Cammi, R.; Pomelli, C.; Ochterski, J. W.; Ayala, P. Y.; Morokuma, K.; Voth, G. A.; Salvador, P.; Dannenberg, J. J.; Zakrzewski, V. G.; Dapprich, S.; Daniels, A. D.; Strain, M. C.; Farkas, O.; Malick, D. K.; Rabuck, A. D.; Raghavachari, K.; Foresman, J. B.; Ortiz, J. V.; Cui, Q.; Baboul, A. G.; Clifford, S.; Cioslowski, J.; Stefanov, B. B.; Liu, G.; Liashenko, A.; Piskorz, P.; Komaromi, I.; Martin, R. L.; Fox, D. J.; Keith, T.; Al-Laham, M. A.; Peng, C. Y.; Nanayakkara, A.; Challacombe, M.; Gill, P. M. W.; Johnson, B.; Chen, W.; Wong, M. W.; Gonzalez, C.; Pople, J. A. *Gaussian 03*, rev. C.; Gaussian, Inc.: Wallingford, CT, 2004.

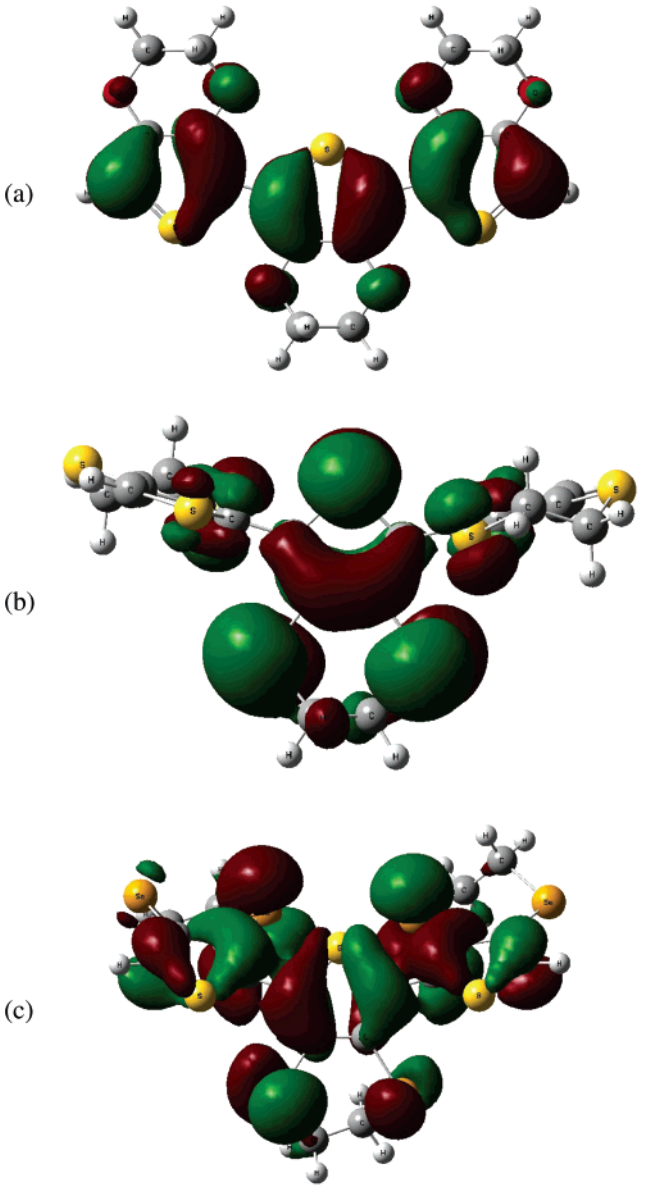

Figure 6. HOMO orbitals (0.02 au isovalue surface) of (a) $(EDOT)_3$, (b) $(EDTT)_3$, and (c) $(EDST)_3$.

explore the thiophene−thiophene torsional potentials in detail at a higher level of theory, which is beyond the scope of the current paper. Whereas the van der Waals contacts must play an important role, there is strong electronic control exerted by orbital interactions. The HOMO for each trimer system is plotted in Figure 6. The top plot shows the $(EDOT)_3$ HOMO, and the planar structure clearly shows the participation of the chalcogen lone pairs in the π system. The middle plot shows the $(EDTT)_3$ HOMO; here, the planes of the two exterior EDTT units are at right angles to the plane of the central unit. By rotating out of the plane, the antibonding interactions with the central thiophene unit are reduced. In $(EDST)_3$ (bottom plot), a nonplanar geometry is adopted that ameliorates the antibonding interactions and stabilizes the HOMO. These orbital interactions we believe are the decisive factors in determining the geometries in the trimer systems.

We next performed 1D band structure calculations on the infinite polymeric systems. To obtain the alternating (anti) orientation of the thiophene units, we extracted a dimer unit from each optimized trimer structure and submitted it for

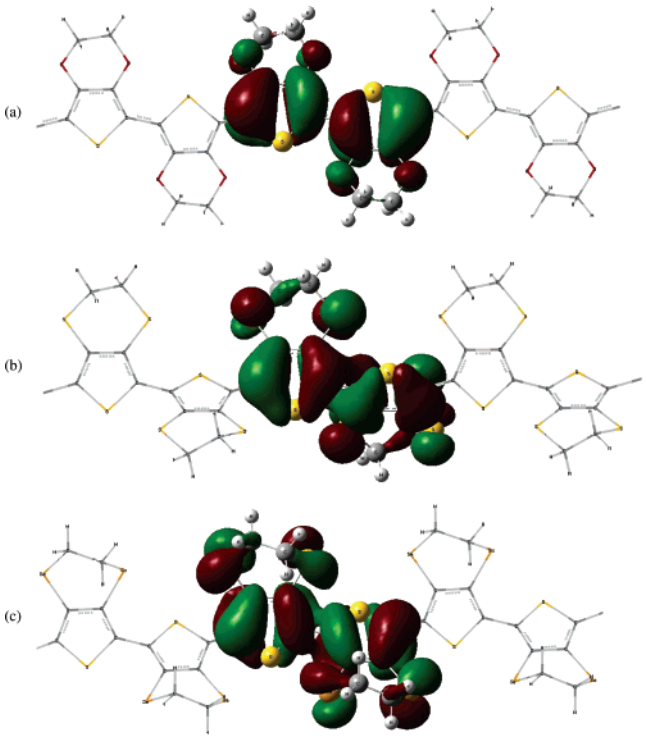

Figure 7. HOMO orbitals (0.02 au isovalue surface) of (a) PEDOT, (b) PEDTT, and (c) PEDST.

full geometry optimization with periodic boundary conditions. Geometrically, PEDOT shows very little difference in structure from $(EDOT)_3$. The dihedral angle between the S atoms of the thiophene units is essentially unchanged, 178 ($(EDOT)_3$) and 179° (PEDOT). Similarly, the S−O contacts discussed above change from 2.96 ($(EDOT)_3$) to 2.94 Å (PEDOT). The band gap, as expected, moves very substantially from 3.30 ($(EDOT)_3$) to 1.83 eV (PEDOT), which is in tolerable agreement with the experimental (absorption spectra on thin films) band gap of 1.63 eV. By contrast, the structure of PEDTT shows a significant change in the dihedral angle between the planes of the thiophene units, 89 ($(EDTT)_3$) to 127° (PEDTT). Accordingly, the S−S contact distance is reduced from 4.09 ($(EDTT)_3$) to 3.44 Å (PEDTT). The band gap is reduced significantly to 3.12 eV but is significantly larger than that obtained from the experiment (2.15 eV). The nonplanar geometry permits favorable (bonding) interactions between the thiophene units (see Figure 7) and stabilizes the HOMO, giving too large a band gap. PEDST mimics PEDTT in that the dihedral angle opens up relative to the trimer, 128 ($(EDST)_3$) and 142° (PEDST), but there is a very small increase in the S−Se contact distance (3.35 Å ($(EDST)_3$), 3.40 Å (PEDST)). The band gap is reduced to 2.67 eV, but as in the case of PEDTT, it is predicted to be significantly larger than the experimental band gap of 1.79 eV.

In principle, it would be useful to carry out 3D band structure calculations to see if the presence of interchain contacts influences the final structures of these systems. There are a number of reasons why this was not done: (i) The cost of band structure calculations is extremely high. (ii)Interchain contacts and the dispersion forces that operate are not well-treated in a density functional formalism; a higher level of theory is required, which would render the

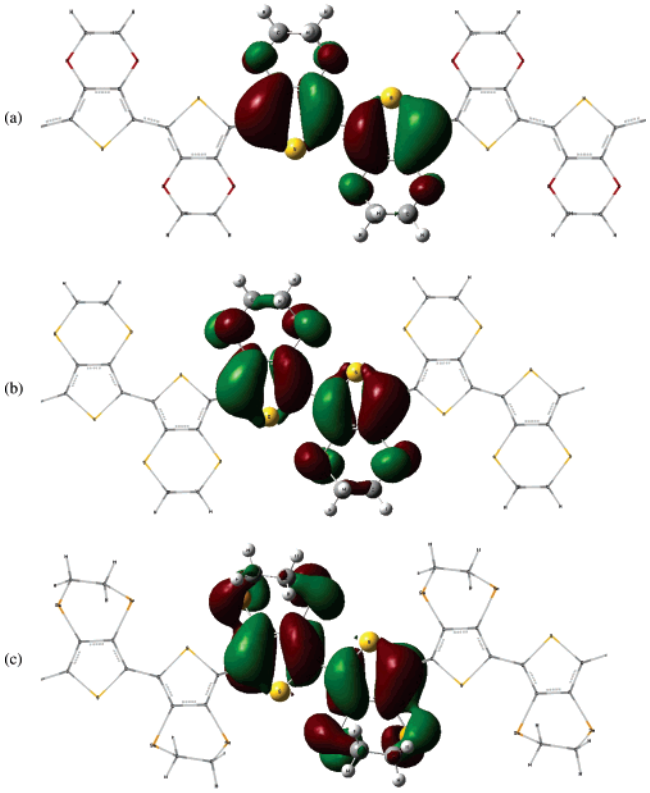

Figure 8. HOMO orbitals (0.02 au isovalue surface) of (a) PEDOT, (b) PEDTT, and (c) PEDST under planar constraint.

calculations intractable. (iii) When moving to 3D, one must address the issue of the polymorphism of how the systems pack; it is to be expected that many potential energy surface minima will exist, and without a supporting X-ray analysis, it would be difficult to ensure that the correct packing was being modeled. These reasons all suggest that full 3D modeling would not yield any sensible insights within a reasonable computational effort.

During the geometry optimizations on PEDTT and PEDST systems, it became evident that the potential energy surface with respect to the interplane dihedral angle is quite flat and that large changes in this geometric variable cause only small shifts in the energy. Hence, we wished to know the energetic cost of imposing a planar structure on these polymeric systems. Additionally, we have shown that the geometric preferences arise from favorable bonding interactions, which stabilize the HOMO. By imposing a planar geometry, we would expect that these favorable interactions are reduced or eliminated. This would lead to a destabilization of the HOMO and a corresponding decrease in the band gap. To this end, we performed geometry optimizations on PEDOT, PEDTT, and PEDST with the single geometric constraint that the dihedral angle between the planes of the thiophene units is exactly 180°. Table 3 shows that under this constraint of planarity, there is a significant decrease in the S−S contact distances in PEDTT and PEDST. PEDOT remains essentially the same, as its structure was already near planar. For PEDTT, the planar constraint costs 19.7 kJ mol^{-1}. This is not a small amount of energy, but significant interchain contacts and other packing forces could provide the necessary energy, at least partially. In the case of PEDST, the move to planarity requires less change in the dihedral angle; when the optimization is converged, we find the planar structure is 13.9 kJ mol^{-1} lower in energy than the previous unconstrained structure. It is in the nature of most optimization algorithms that they converge to the stationary point nearest to the starting geometry, and the previous geometry optimizations were started from the gas-phase trimer geometries. To confirm the lowering of energy obtained for PEDST under planar constraint, we repeated the optimization starting from the planar geometry but without any constraints. The final structure obtained has a dihedral angle between the thiophene units of 177°, the energy is lowered by only 0.1 kJ mol^{-1}, and the band gap is unaltered. In the case of PEDTT, the HOMO (under planar constraint, see Figure 8) loses its bonding interactions between units and the energy rises. In the case of PEDST, the bonding interactions between rings are again removed, but the Se atom, being larger and more diffuse than the S atom, is able to produce a favorable bonding interaction within each unit, as shown in Figure 8c (see bottom right and top left). The predicted band gaps are now 2.07 (B3LYP/6-31G(d)) and 2.15 eV (experiment) for PEDTT and 1.86 (B3LYP/6-31G(d)) and 1.79 eV (experiment) for PEDST. This good agreement and its rationalization by Figures 7 and 8 leads us to predict a planar (or very near planar) structure for PEDST.

In summary, we have presented the synthesis and key properties of poly(3,4-ethylenediselenathiophene), the selenium analogue of the well-known conjugated polymer PEDOT. Experimental data and computational results indicate that PEDST adopts a far more planar structure than PEDTT and that its band gap is closer to that of PEDOT. Because of the lower LUMO of PEDST (with respect to PEDOT and PEDTT), the incorporation of EDST into copolymers can be envisaged as a means to improve electron tranport in the parent polymer or to improve the efficiency in bulk heterojunction organic solar cells.[28] Further investigations are under way to elucidate the electronic and structural properties in the latest of this fascinating series of chalcogen-rich polymers.

Acknowledgment. P.J.S. thanks the Leverhulme Trust for a Research Fellowship.

CM062242P

(28) Scharber, M. C.; Wuhlbacher, D.; Koppe, M.; Denk, P.; Waldauf, C.; Heeger, A. J.; Brabec, C. L. *Adv. Mater.* **2006**, *18*, 789.